



# The Role of Chitosan (CHS) and Chitosan-Silver Nanoadsorbents (COMP) in Adsorption of Cu (II) and Fe (II) Ions from Electroplating Wastewater

A Sumaila<sup>1,2\*</sup>, MM Ndamitso<sup>1</sup>, YA Iyaka<sup>1</sup>, AS Abdulkareem<sup>3</sup> and JO Tijani<sup>1</sup>

<sup>1</sup>Department of Chemistry, Federal University of Technology Minna, Niger State, Nigeria

<sup>2</sup>Department of Pure and Industrial Chemistry, Kogi State University Anyigba, Kogi State, Nigeria

<sup>3</sup>Department of Chemical Engineering, Federal University of Technology Minna, Niger State, Nigeria



## Abstract

In this work, green development of CHS-silver nanocomposite (COMP) using aqueous leaf extracts of *Nicotiana tabacum* and silver nitrate as reducing agent and precursor respectively. The prepared CHS and COMP were characterized by ultraviolet-visible (UV-Vis) spectroscopy, X-ray diffraction (XRD) and Fourier Transform Infrared (FTIR) Spectroscopy. The CHS and nanocomposite were employed to remove copper and iron metal ions from electroplating wastewater via batch adsorptions process. The XRD results of the nanocomposite confirmed the formation of COMP. The BET results showed increased in surface area of CHS from 12.67 to 139.20 m<sup>2</sup>/g after doped with nanosilver. The maximum percentage removal of copper and iron by COMP were 94.76% and 98.80% respectively under the applied conditions of 348 K (temperature), 60 minutes (contact time) using 25 mg (adsorbent dosage). The isotherm data were well best fitted to Jovanovic isotherm model. While kinetic data followed the pseudo-second order model, an indication of chemical adsorption. This study showed that COMP with high adsorption efficiency can be used successfully to adsorbed copper and iron from electroplating wastewater.

## Keywords

*Nicotiana tabacum*, Electroplating wastewater, Adsorption, Crab shell, Nanocomposite

## Introduction

The contamination of environment by potentially toxic metals is one of the foremost hazards threatening human and aquatic species, thus the need for urgent attention on how to curb it [1]. These toxic metals find their way into the environment through release of geogenic, industrial, agricultural, pharmaceutical, and domestic wastewater. Through food chain, the heavy metals enter and accumulate in living tissues and become detrimental to human health [2,3]. Exposure to dose of heavy metals can result to damage or failure of essential human organs such as liver; kidney, cancer and brain [3]. In view of this, heavy metal ions must be removed prior to discharge into water bodies.

Electroplating wastewater as an industrial wastewater is a large volume of wastewater discharge from electroplating process. This industrial wastewater can be acidic or alkaline, depends on the nature of production however contain heavy metals usually at elevated levels according to the kind of metal solution used in the process [4]. Among the heavy metals usually present in electroplating wastewater are copper and iron. The presence of high amount of these metals has been

reported to cause health disorderliness range from stomach ache to liver to damage [3]. Hence, their release to the environment is disastrous to human life, it is therefore important that electroplating wastewater be adequately treated using suitable treatment technique before discharge into the environment.

Over the years, there have been series techniques employed to remove heavy metals from electroplating wastewater [5]. Prominent among these techniques are co-precipitation, precipitation, reverse osmosis, chemical coagula-

**\*Corresponding author:** A Sumaila, Department of Chemistry, Federal University of Technology Minna, Niger State; Department of Pure and Industrial Chemistry, Kogi State University Anyigba, Kogi State, Nigeria

**Accepted:** November 05, 2020

**Published online:** November 07, 2020

**Citation:** Sumaila A, Ndamitso MM, Iyaka YA, et al. (2020) The Role of Chitosan (CHS) and Chitosan-Silver Nanoadsorbents (COMP) in Adsorption of Cu (II) and Fe (II) Ions from Electroplating Wastewater. *Adv Environ Stud* 4(2):318-330

tion, electrodialysis, flocculation, membrane separation and ion-exchange [6]. Nevertheless, these methods often involve certain major limitations such as high energy needs, inefficient metal removal, and production of a large amount of toxic waste, cost of operation, complex reaction and uses of heavy chemicals [7]. The process of adsorption using biomaterials to remove heavy metals from industrial wastewater is considered to be a simple and effective technique in wastewater management [8]. Numerous studies have shown the potential to use these materials to remove heavy metal ions from industrial wastewater due to their effectiveness, low cost, biodegradability and large-scale use [9].

Biomaterials, particularly those of shellfishes are generated in large quantities as waste [10]. These wastes are biodegradable, their careless disposals in large quantities result to accumulation of wastes in public waters and landfills, and if left for a while, they decomposed causing odours which impair soil and water quality [11]. Thus, they can be converted into useful adsorbent like CHS.

Meanwhile, sequestrations of heavy metals from environment particularly water bodies using CHS have been studied by numerous researchers [9]. The removal of Cu (II) ion onto locally prepared and industrial CHS was investigated by [7]. Also, the potential of CHS for the adsorption of selected metal ions ( $Pb^{2+}$ ,  $Fe^{2+}$  and  $Cu^{2+}$ ) from aqueous solutions was studied by Sobhanardakani, *et al.*, [12]. Despite the fact that there are existing works relating to the use of CHS prepared from sea shells as adsorbents for removal of toxic metals from wastewater, the green preparation of CHS-silver nanocomposites and its use as adsorbent has not been extensively addressed. This article therefore examines this aspect of the production of CHS-silver nanocomposites and then studies its absorption behaviour to adsorb  $Fe^{2+}$  and  $Cu^{2+}$  ions from electroplating wastewater through batch-wise experimental processes.

## Materials and Methods

### Materials

*Nicotiana tabacum* leaves were obtained from a vegetable plantation in Paiko Tunga Awuje in the state of Niger, Nigeria. Crab shells were obtained from fish market in New Bussau Nigeria. All the chemicals used in this study were of analytical grade. The wastewater was obtained from electroplating plant in Nigeria.

### Method

**Extraction of CHS from Crab Shells:** The production of CHS from the powdered crab shells was carried out via three main stages of extraction: Deproteinization, demineralization and deacetylation. The crab shells were deproteinized by treating 5 grams of the crab shells in 250 cm<sup>3</sup> beaker using 1.25M NaOH for 3 hrs at room temperature. After which the mixtures was allow to settle; excess NaOH was filtered off and then washed with deionized water until neutral pH. Filtration was done using Whatmann filter paper No 4, the residue were oven dried at temperature of 80 °C for 45 minutes to obtain deproteinized crab shells.

In the case of demineralization of the deproteinized crab

shells, 3 grams of the deproteinized crab shells was treated in 250 cm<sup>3</sup> conical flask using 1.25M of HCl for 5 hrs at temperature of 80 °C. After heating, the mixtures was allow to cooled and settled; excess HCl was removed by decantation, then washed with deionized water until neutral pH. This was subsequently filtered using Whatmann filter paper No 4 and the residues obtained were oven dried at 80 °C for 45 minutes to obtain chitin.

To carry out the deacetylation of the obtained chitin to produce CHS, 1 gram of the chitin in 100 cm<sup>3</sup> beakers was treated using 0.5M of NaOH for 2 hrs at temperature of 100 °C. After heating, the mixture was allow to cooled and settled; The excess NaOH was removed by decantation, then rinsed with deionized water until neutral pH. After then, it was filtered using Whatman filter paper No. 4, the residue was dried in an oven at 80 °C for 45 minutes to obtain CHS.

**Preparation of aqueous leaf extract of *Nicotiana tabacum*:** Fresh leaves of *Nicotiana tabacum* were washed with distilled water, dried in the sun and then finely ground. 10 g of ground leaf was added to 100 cm<sup>3</sup> of distilled water, boiled in a water bath at 80 °C for 15 minutes, then cooled and filtered through Whatman No. 1 filter paper, then stored at room temperature for further use. The phytochemical analysis was conducted on the extract to determine the presence of phenolic compounds.

**Development of COMP:** COMP was developed by mixing 40 cm<sup>3</sup> of 1M AgNO<sub>3</sub> and 40 cm<sup>3</sup> of 1.0 wt% CHS solutions in a 100 cm<sup>3</sup> conical flasks. This followed by addition of 5 cm<sup>3</sup> aqueous leaf extract of *Nicotiana tabacum* and stirred on a magnetic stirrer at 250 rpm for 2 h and then allowed to age for 24 h. The reduction of silver nitrate to nanosilver was observed using an Ultraviolet-visible spectrophotometer-1800 series. The obtained COMP was lyophilized at 42 °C, which was then stored for further characterization.

**Characterization of the CHS and COMP:** The formation of nanosilver in the COMP was determined an Ultraviolet-visible spectrophotometer-1800 series. The phase structure, surface morphologies, functional groups present and surface area/pore of the prepared CHS and COMP were examined using XRD-6000 Shimadzu Scientific Instruments, Zeiss Auriga High Resolution Scanning Electron Microscope (HRSEM), Frontier FT-IR Perkin Elmer, UK and Brunauer Emmett Teller (BET) respectively.

**Batch adsorption studies:** The concentrations of Cu and Fe ions in the wastewater before and after adsorption were determined using Atomic absorption spectrophotometer (AAS) (Bulk Scientific AAS: Model Accusys 211 USA. Adsorption activities of the adsorbents (CHS and COMP) were evaluated at different contact time, adsorbent dosage and temperature using 50 cm<sup>3</sup> of the electroplating wastewater and stirring speed of 200 rpm. After adsorption, the mixtures were filtered with Whatmann filter paper No 4 and the amounts of the heavy metals remaining in the wastewater were determined using AAS.

**Determination of influence of contact time on the adsorption process:** The influence of contact time on the ad-

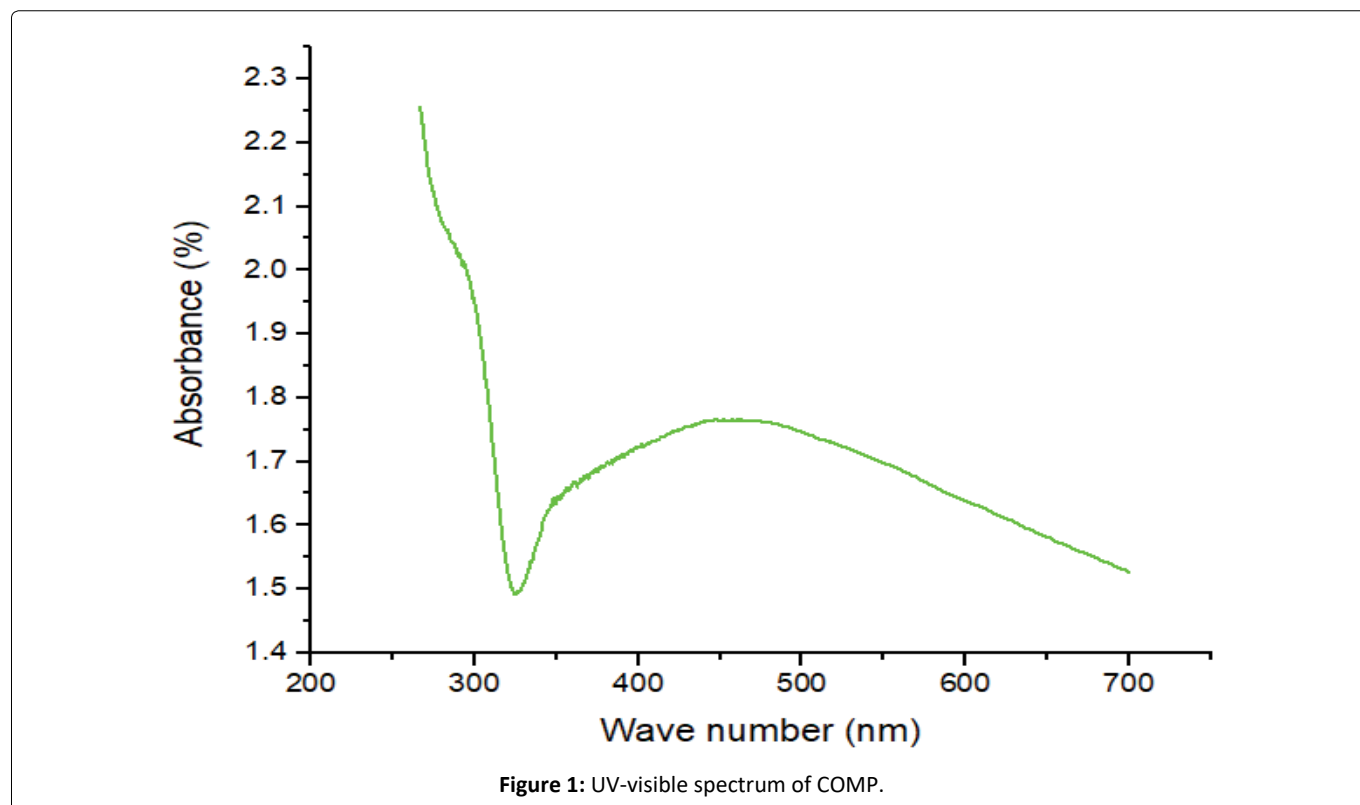


Figure 1: UV-visible spectrum of COMP.

sorption of Cu and Fe from the electroplating wastewater was investigated by contacting 25 mg of adsorbent dosage of the adsorbents with 50 cm<sup>3</sup> of the wastewater agitated at speed of 200 rpm for 15, 30, 45, 60, 75 minutes at room temperature. The adsorbents were separated from the mixtures by centrifugation and the supernatants were analyzed for the residual concentrations of heavy metal ions using AAS.

**Determination of influence of adsorbent dose on the adsorption process:** The adsorptions of Cu and Fe by CHS and COMP were studied at room temperature using different adsorbent dosages of 5, 10, 15, 20 and 25 mg and 50 cm<sup>3</sup> of electroplating wastewater for optimum contact time at stirring speed of 200 rpm. The adsorbents were removed from the solution by centrifugation and the supernatants were analyzed for the residual concentrations of Cu and Fe ions using AAS.

**Determination of influence of temperature on the adsorption process:** The optimum adsorbent dosage obtained was taken to monitor the effect of temperature on adsorption process. The adsorption experiments were carried out at different temperature of 303, 318, 333, 348 and 363 K with an optimum adsorbent dosage established and agitated at speed of 200 rpm. The adsorbents were separated from the mixtures by centrifugation and the supernatants were analyzed for the residual concentrations of Cu and Fe ions using AAS.

**Data analysis:** The equation 1 was employed to determine the amount of Cu and Fe ions removed.

$$q_e = \frac{(C_o - C_e)V}{m} \quad (1)$$

Implies that C<sub>o</sub> and C<sub>e</sub> are amounts (mg/l) of the selected

metal ions before and after removal, respectively, V is the volume of wastewater in cm<sup>3</sup> and m is the dose of the adsorbents in grams.

$$\text{Removal}(\%) = \frac{C_o - C_e}{C_o} \times 100 \quad (2)$$

The equation 2 was employed to determine the percentage removal of the selected metal ions. Where C<sub>o</sub> is the initial concentration of heavy metals (mg/dm<sup>3</sup>), C<sub>e</sub> is the equilibrium concentration of the heavy metals (mg/dm<sup>3</sup>), and R is the adsorption percentage. All the model parameters were evaluated by linear regression using Microsoft Excel. Apart from the correlation coefficient (R<sup>2</sup>), standard error (S.E) was also used to measure the goodness-of-fit. The smaller S.E. value indicates the better curve fitting.

## Results and Discussions

### UV-visible spectroscopy analysis of CHS and COMP

The formation of nanosilver by reduction of Ag<sup>+</sup> ions was observed by UV-visible spectroscopy. During the reduction process, the colourless CHS solution containing AgNO<sub>3</sub> gradually turned brown, signifying the transformation of Ag<sup>+</sup> into Ag<sup>0</sup> [13]. The presence of nanosilver in the composite material was confirmed by the UV-visible spectrum (Figure 1) with a maximum absorption band at 447 nm, which is in the range of the typical plasmon resonance band of nanosilver [13] as shown on the UV-visible spectrum of COMP in Figure 1.

### FTIR of CHS and COMP

The FTIR spectrum of the CHS (Figure 2a) showed peaks

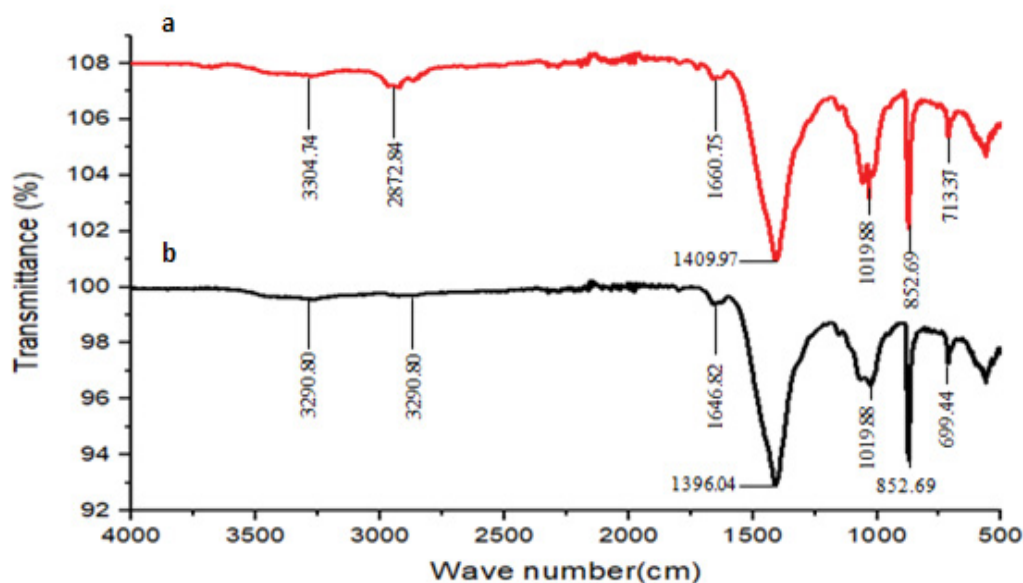


Figure 2: FTIR of (a) CHS; (b) COMP.

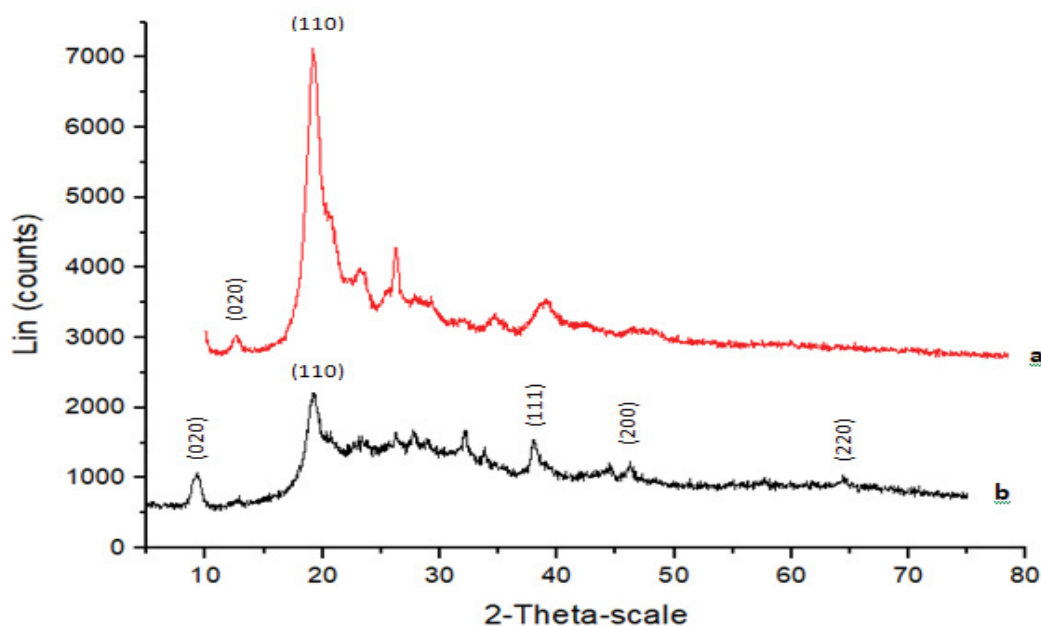


Figure 3: Diffractogram of (a) CHS; (b) COMP.

at 3304.74, 2872.84, 1660.75, 1409.97, 1033.81, 866.62 and 713.37  $\text{cm}^{-1}$ . The absorption peak at 3304.74  $\text{cm}^{-1}$  is attributed to the overlapped peaks of the N-H and O-H stretching vibration [14]. The absorbance peaks at 2872.84  $\text{cm}^{-1}$ , 1660.75  $\text{cm}^{-1}$  and 1409.97  $\text{cm}^{-1}$  indicate the C-H stretching of polymeric link, N-H in-plane bend and O-H deformation in-plane respectively [15]. The characteristic absorption peaks at 1033.81 and 866.62  $\text{cm}^{-1}$  are attributed to C-O stretching of O-H groups due to deformation [16-18]. The peak observed at 713.37  $\text{cm}^{-1}$  is attributed to N-H [17].

From the FTIR spectrum (Figure 2b) of the COMP, it is observed that the nanocomposites show similar surface func-

tional groups which are alike to that shown by CHS. However, all the nanocomposites have it absorption intensities varied and frequencies of O-H deformation in-plane and N-H in-plane bending shifted. This trend displayed by the nanocomposites shows a successful coordination of -OH and -NH<sub>2</sub> of CHS with the silver metal center and indicates that the silver nanoparticles were successfully linked onto the CHS polymer matrix via similar coordination manners of the silver nanoparticle [19]. Though, the shifting in frequencies to lower or higher wave numbers as well as the change in the absorption intensities are attributed to the ratio of silver ion to CHS in the nanocomposites [20].

### XRD Results of CHS and COMP

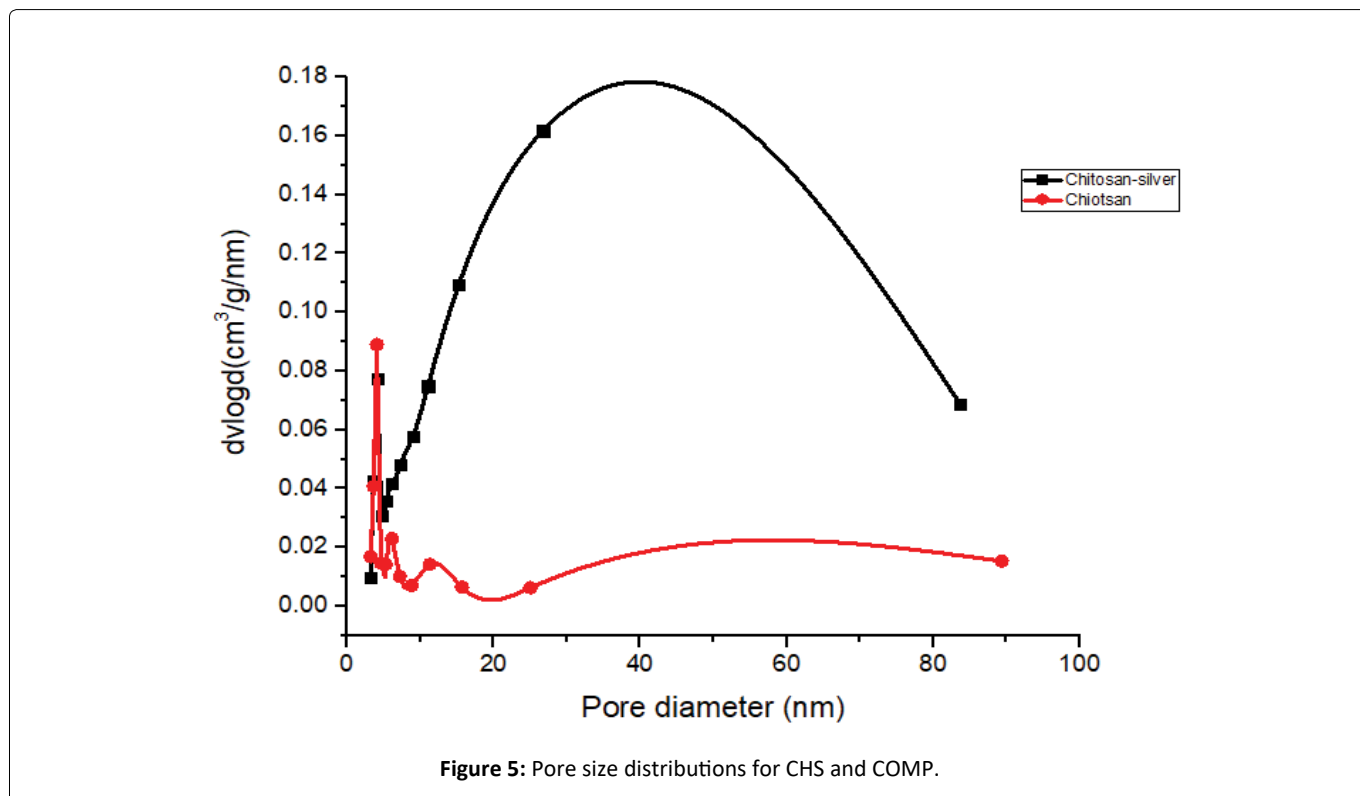
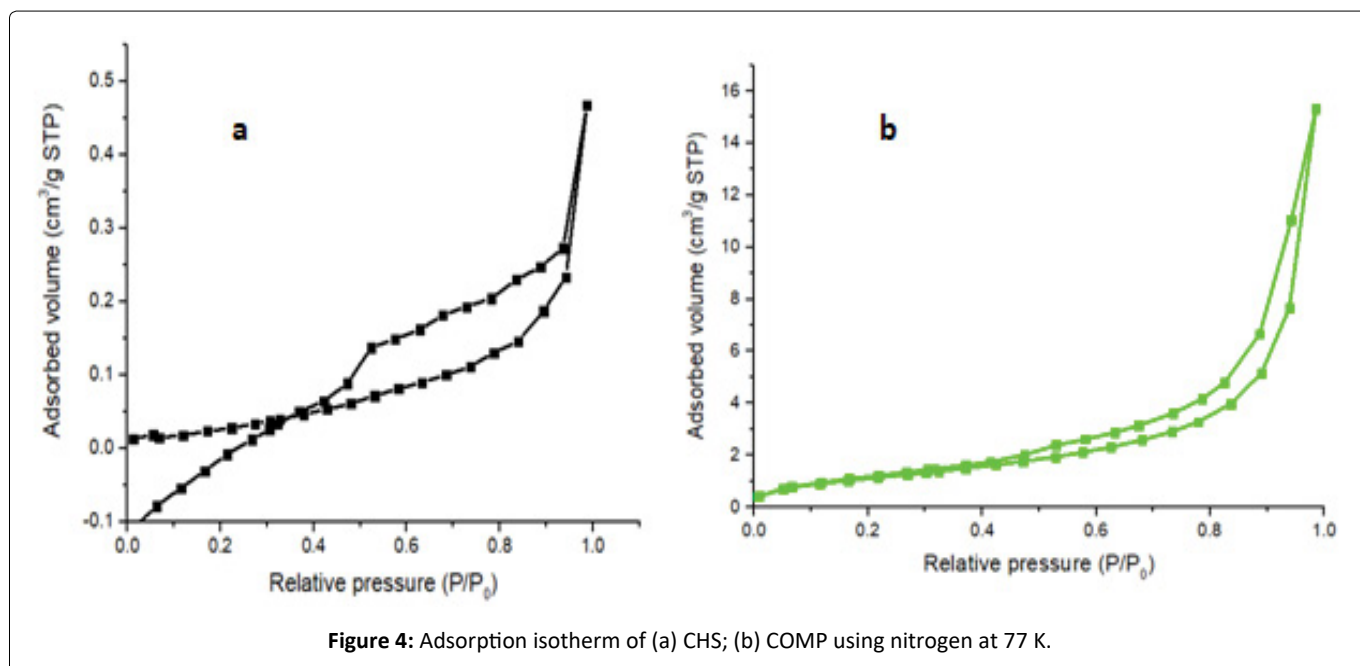
XRD technique was employed to investigate the phase formations of the both CHS and COMP and the diffractogram are displayed as Figure 3a and Figure 3b respectively. The significant peaks at  $2\theta$  of  $12.56^\circ$  and  $19.20^\circ$  showed in Figure 3a which correspond with crystal planes (020) and (110) are usually of semi-crystalline CHS. Also, the diffraction peaks at  $9.29^\circ$  and  $19.30^\circ$  with crystal planes (020) and (110) in Figure 3b matched well with XRD pattern of CHS. In the same vein, Figure 3b shows weak but sharp diffraction peaks at  $2\theta$  of  $38.04^\circ$ ,  $44.65^\circ$  and  $64.45^\circ$  assigned (111), (200) and

(220). These diffraction peaks matched well with that of silver nanoparticles [21]. While other peaks may be originated from the molecules of leaf extract [22].

### BET of CHS and COMP

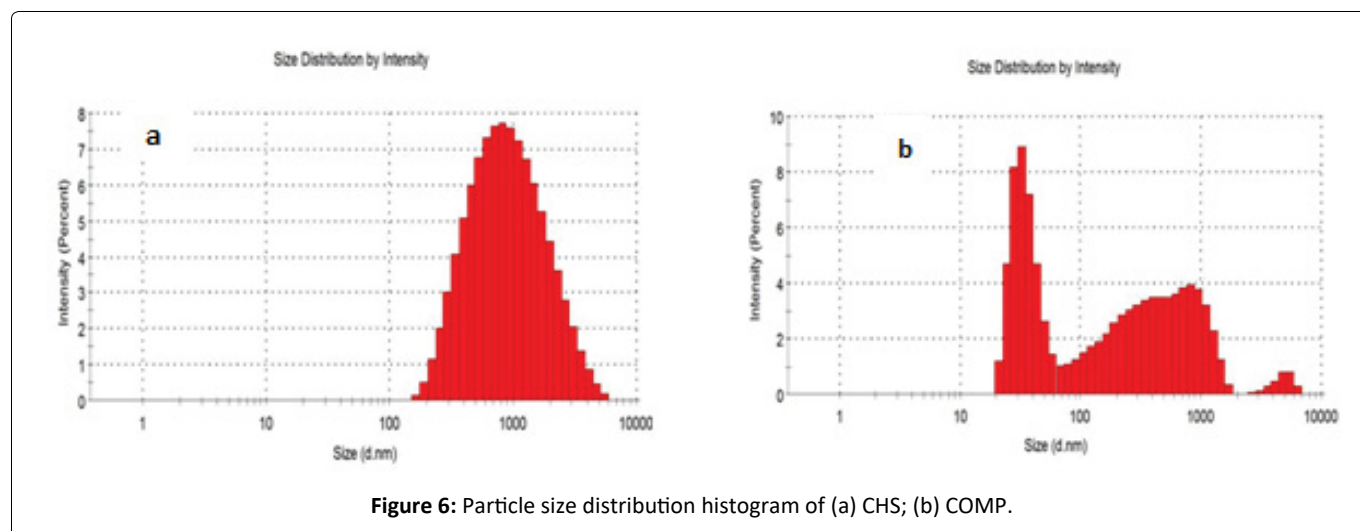
Determination of specific surface areas, pore sizes and pore volumes of the CHS and COMP were carried out by nitrogen gas adsorption-desorption at 77 K. Specific total surface areas were determined using the Brunauer Emmett Teller (BET) (Figure 4 and Figure 5).

Table 1 shows that the surface area, pore volume and



**Table 1:** Results of BET analysis of CHS and COMP.

S/N	Material	Surface area (m <sup>2</sup> /g)	Pore volume (cm <sup>3</sup> /g)	Pore size (nm)
1	CHS	12.67	0.0266	4.035
2	COMP	33.46	0.1347	4.078



**Figure 6:** Particle size distribution histogram of (a) CHS; (b) COMP.

pore size of CHS increased from 12.67 m<sup>2</sup>/g to 33.46 m<sup>2</sup>/g, 0.0266 cm<sup>3</sup>/g to 0.1347 cm<sup>3</sup>/g and 4.035 nm to 4.078 nm respectively after incorporation with silver to form the nanocomposite of CHS-silver. This may be attributed to reduction of agglomeration of CHS due to the presence of nanoparticles of silver in the polymer matrix of CHS. The specific surface area of CHS in this work is higher than the 0.1698 m<sup>2</sup>/g and 5.5156 m<sup>2</sup>/g obtained by Thien, *et al.*, [23] for bare CHS and fully deacetylated CHS respectively. In this vein, the pore volume of the prepared CHS increased after loaded with silver. This result is agreed with the results reported by Razzaz, *et al.*, [24] on CHS nanofibers functionalized by TiO<sub>2</sub> nanoparticles for the removal of heavy metal ions. According to International Union of Pure and Applied Chemistry (IUPAC) pores are classified based on diameter, for instance macropores (d > 50 nm), mesopores (2 < d < 50 nm) and micropores (d < 2 nm). Therefore, CHS, and COMP are mesoporous in nature.

### Dynamic light scattering of CHS and COMP

Intensity particle size distribution histogram of CHS and COMP in Figures 6a and Figures 6b indicate that 100% of particle sizes of CHS is within the range of 100-10000 nm, with average particle size of 729 nm, while that of COMP shows two major peaks: First peak which falls within 10-100 nm reveals the presence of nanosilver of mean size of 35.71 nm; second peak within 100-1000 nm indicates CHS of reduced particle sizes of mean size of 360.4 nm. The high average particle size of CHS obtained in this study may be attributed to the absence of electrostatic hindrance to the repulsion between protonated amino groups [25]. From Table 2, CHS mean particle size was 729 nm and latter reduced to 360.4 nm after incorporation of nanosilver. This may be attributed to increase in protonation of amino group, increasing the propensity of CHS cross-linking, resulting in a more compressed structure due to creation of electrostatic repulsion [26].

**Table 2:** DLS results of CHS and COMP.

Parameter	CHS	COMP
Average particle size (nm)	729	360.4
Polydispersity index	0.275	0.388

Also, Table 2 shows the polydispersity indices (PDI) for CHS and COMP to be 0.275 and 0.388 respectively, these are within the range of 0.1-0.4 indicating that particles of CHS and its nanocomposite are moderately polydisperse but having that of composite particles to be more polydisperse.

### High resolution scanning electron micrographs (HRSEM) of CHS and COMP

Figure 7a and Figure 7b shows the HRSEM micrographs of CHS and COMP. The CHS micrograph shows needle-like crystalline structure with smooth surface as fine powder. While, after doped with silver nanoparticles due to agglomeration of the nanosilver, the surface becomes rough and porous with crystals-like silver nanoparticles seen evenly distributed across the surface (Figure 7b), this trend is aligned with result from previous study [27]. The needle-like structure obtained for CHS is aligning with what Krishnaveni and Ragunathan [28] obtained as the morphology of CHS. Further proof to the combination of nanosilver and CHS was shown on electron dispersive spectra (EDS) presented in Figure 7b. Hydrogen being the only element in the periodic table with only K-shell is not detectable with EDS [29].

Figure 8a and Figure 8b is the EDS and elemental composition histograms of CHS and CHS-silver spectrum showing the key elements (carbon, nitrogen and oxygen) and (C, N, O and Ag) on the surface chemical structure of the samples respectively. The presence of Na and Si signals may be attributed to strong bond formed by Na as micronutrient commonly found

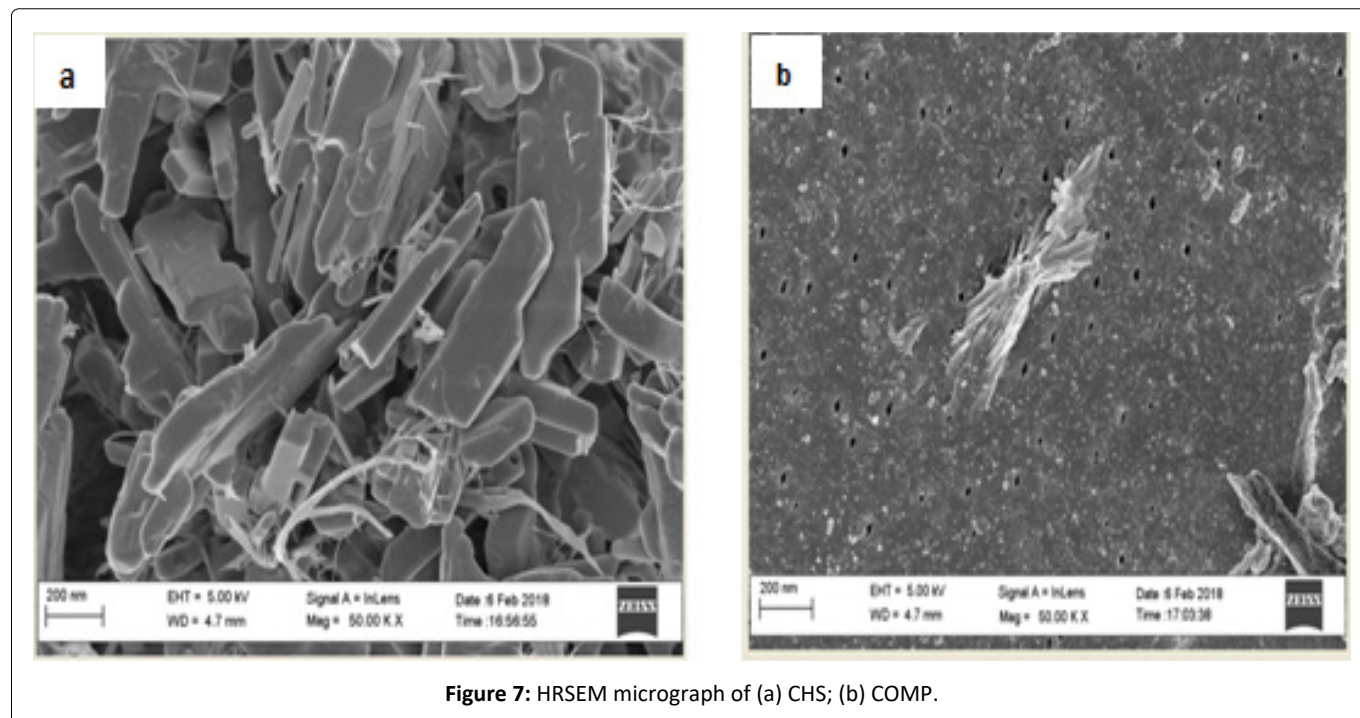


Figure 7: HRSEM micrograph of (a) CHS; (b) COMP.

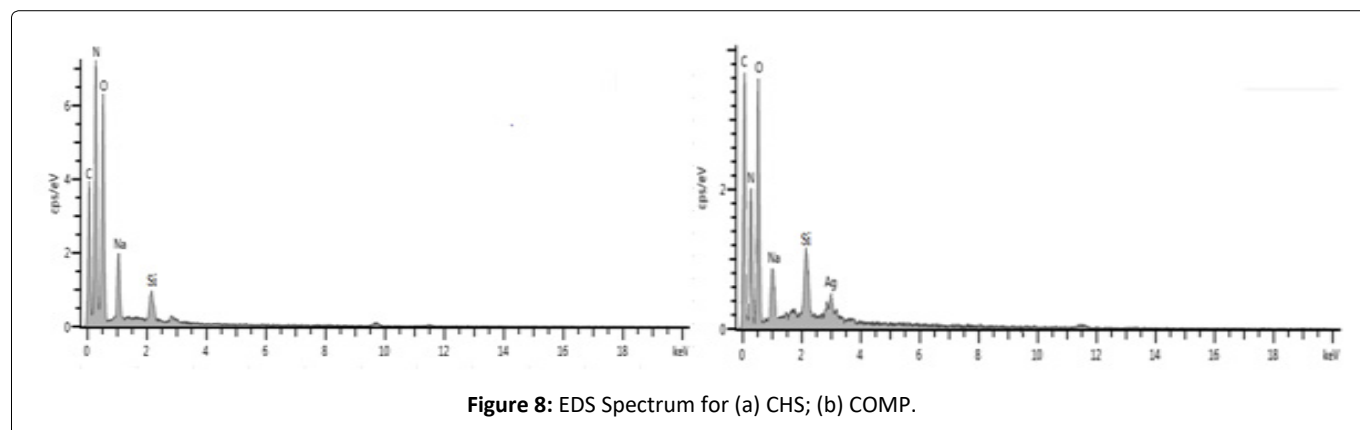


Figure 8: EDS Spectrum for (a) CHS; (b) COMP.

in both CHS and plant extracts and to interferences of debris of silicon-lithium detector as component of the machine used, due to prolonged usage respectively.

### Batch adsorption of heavy metals in electroplating wastewater

The CHS and COMP produced were employed to treat wastewater from electroplating plant. The influences of contact time, adsorbent dose and temperature on the adsorption of the selected metal ions by developed adsorbents were investigated and the results obtained are hereby presented as follows.

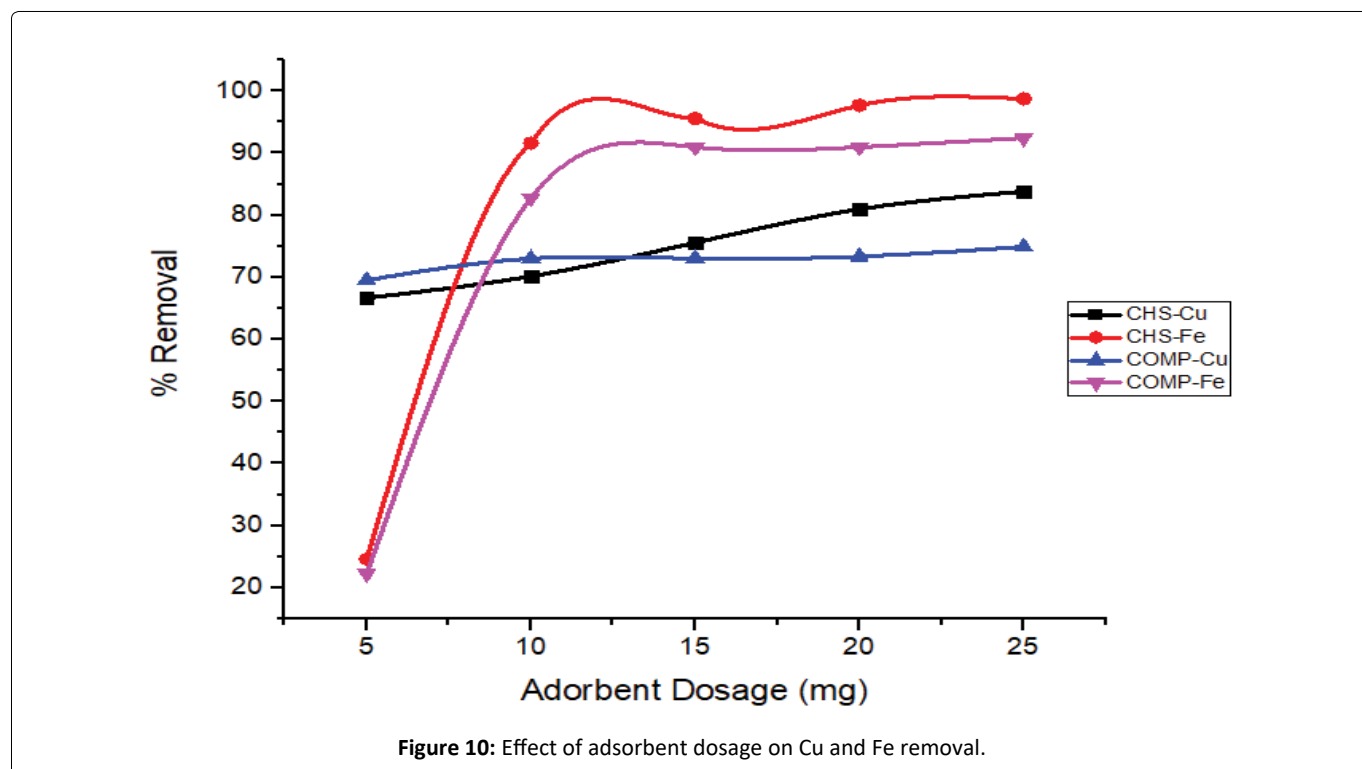
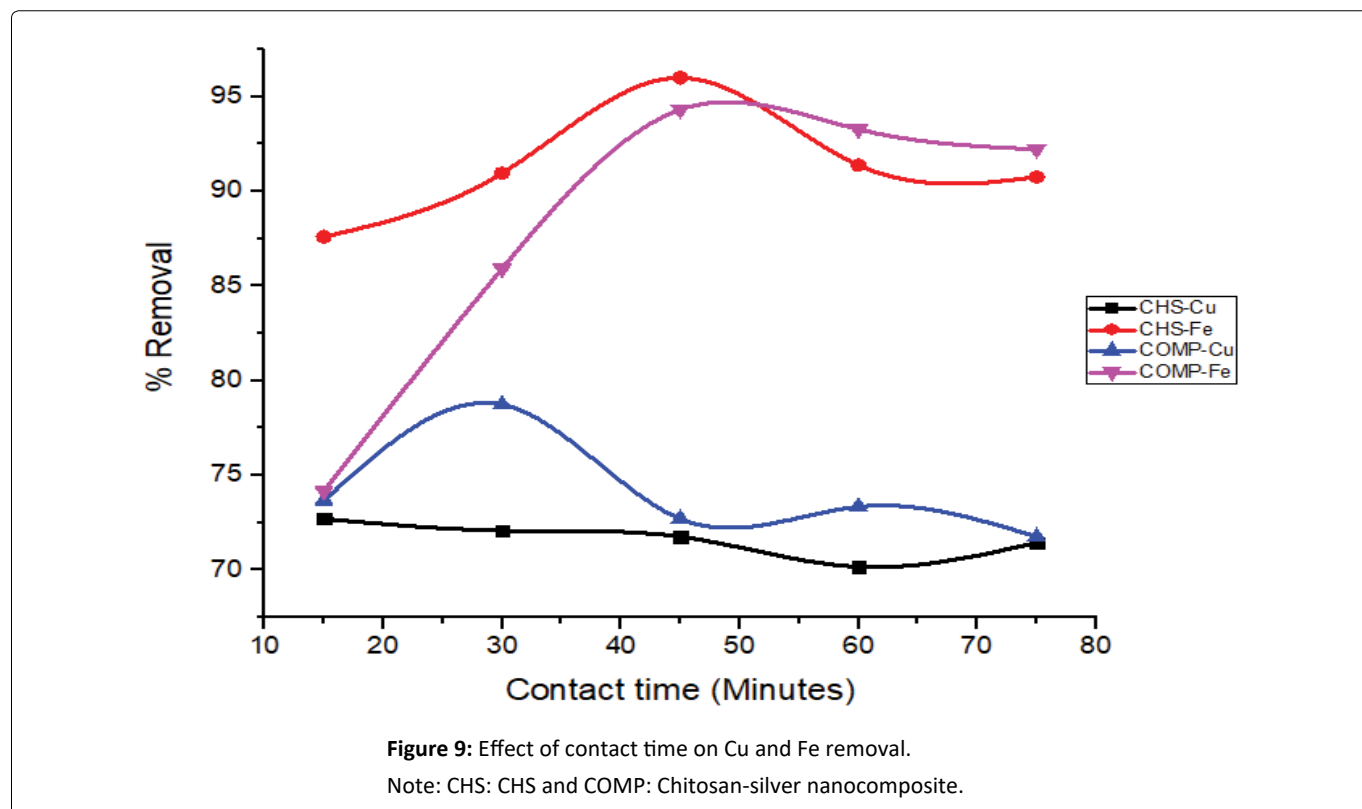
**Influence of contact time on the removal of Cu and Fe ions:** Figure 9 represents the influences of contact time on the percentage uptake of Cu and Fe ions by CHS and COMP (volume = 50 cm<sup>3</sup>, adsorbent dosage = 25 mg, temperature = 30 °C, stirring speed = 200 rpm).

The relationship between the percentage removals of metal ions with the contact time, as shown in Figure 9, shows that both adsorbents initial removal of Cu and Fe ions from

wastewater very fast. The optimum contact time for the removal of Fe ions by CHS and COMP was 45 minutes while the optimum percentage removals of Cu ions on both adsorbents was attained in about 30 minutes. The initial fast rate of removal of both metal ions can be attributed to the initial large availability of a number of binding sites on the adsorbents, while later slow removal rate may be due to weak interaction between the adsorbates and the adsorbents as a result of a reduction in the number of binding sites [30]. It is thus obvious from Figure 9 that in a little time the proportion of both metal ions removed on the adsorbent was high. This can be due to the fact that more metal ions were available which encourage quick diffusion the ions from the wastewater to the free active sites on the adsorbents [31].

**Influence of adsorbent dose on the removal of Cu and Fe ions:** The amount of adsorbent played an important role in an adsorption process, as it describes the adsorbent's ability to remove metal ions in terms of the number of active binding sites.

As shown in Figure 10, the proportion of both ions re-



removed increases with the dose of adsorbents (5 to 25 mg). This high removal of the metal ions may be as a result of the presence of more binding sites as the dose of adsorbent increased [32]. The initial percentage removal of Fe ions on both adsorbents was lower compared to Cu ions due to latter smaller ionic radius but as dosage increased the affinity of both adsorbents for Fe ions rise so leads to higher adsorption [33]. This result is consistent with the result obtained by

Priyanka, *et al.* [34] on the adsorption of Pb (II), Cu (II), and Zn (II) ions on the leaves of *Urtica dioica* as an inexpensive adsorbent.

**Influence of temperature on the removal of Cu and Fe ions:** The influence of change in temperature on the uptake of Cu and Fe ions by CHS and COMP at constant adsorbent dose, contact time and stirring speed was studied (Figure 11).

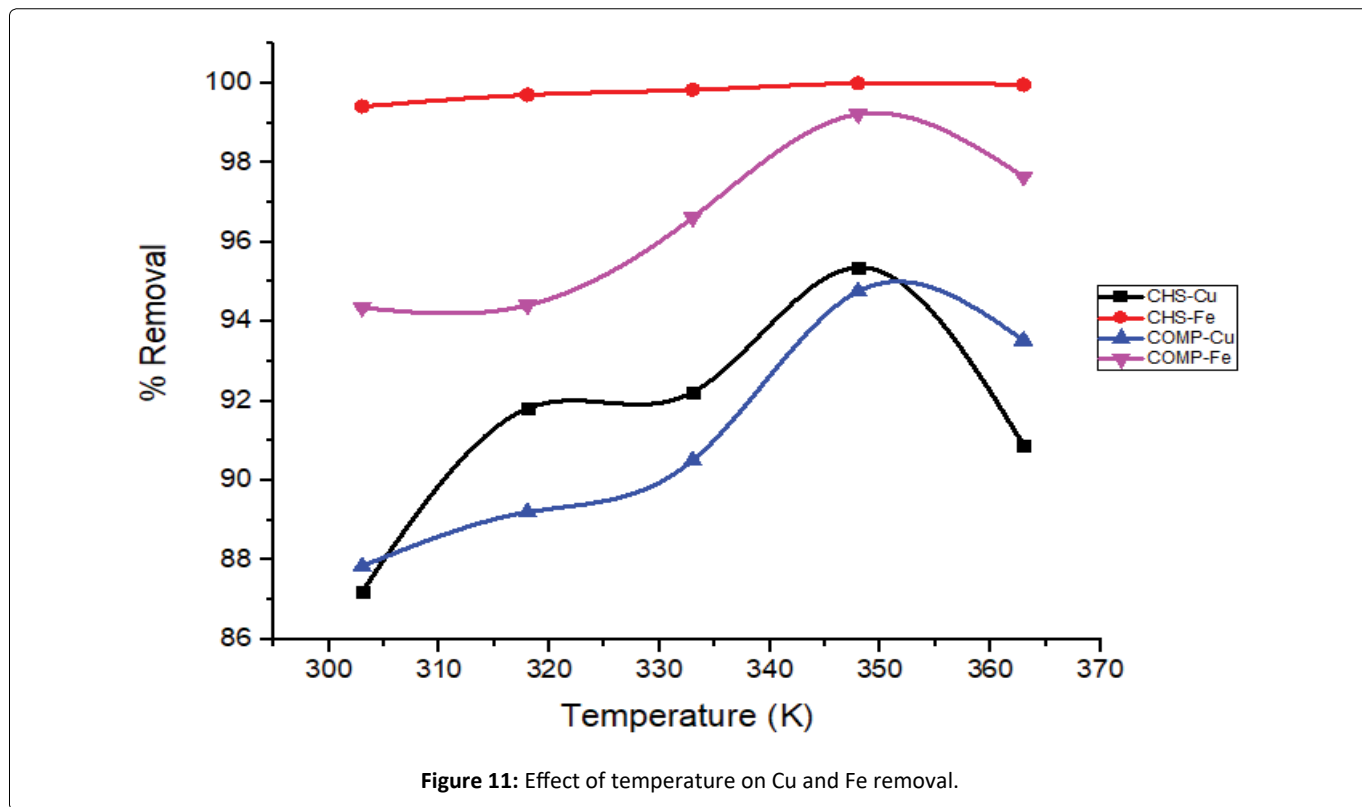


Figure 11: Effect of temperature on Cu and Fe removal.

Table 3: Details of variables plots for the isotherm models.

Isotherm model	Dependent variable	Independent variable	Slope	Intercept
Freundlich	$\ln q_e$	$\ln C_e$	$1/n$	$\ln K_f$
Jovanovic	$\ln q_e$	$C_e$	$-K_j$	$\ln q_{max}$
Harkin – Jura	$1/q_e^2$	$\text{Log} C_e$	$-1/A_{HJ}$	$B_{HJ}/A_{HJ}$
Temkin	$q_e$	$\ln C_e$	$K_1$	$K_1 \ln K_2$

From Figure 11 it is observed that the percentage uptake of Cu and Fe ions by CHS and COMP increased respectively as temperature rise from 303 to 348 K. These outcomes concurred with the findings of [35] on the removal of  $\text{Cu}^{2+}$  by activated carbon produced from grape bagasse. This study shows that the removal of Fe ions by CHS was significantly influenced by the change in temperature compared to COMP.

Generally, increased temperature is expected to significantly induce the adsorption of metal ions by adsorbents, easing more binding sites and movement of the adsorbates from the bulky aqueous medium to the adsorbent binding sites [36]. But in this study, the adsorption of Cu and Fe ions by CHS and COMP at a lower temperature of 303 K was initially fast and later became slowly as temperature increased. This is supported by the result reported by Md. Sayedur and Katherine [37] on metal ions removal from aqueous solutions by *Kappaphycus sp.*

**Isotherm Models of Cu and Fe ions Adsorption:** In this study, four isotherm models were adopted: Freundlich, Jovanovich, Harkin Jura and Temkin Isotherm. Using adsorption data obtained, the isotherms were plotted linearly and the constants, standard errors, and correlation coefficients ( $R^2$ ) of the model were calculated. The fitness of adsorption data

into the selected isotherm models was checked using  $R^2$  and standard error values. The relationship presented in Equations 3, 4, 5 and 6 represent Freundlich, Harkins-Jura, Jovanovic and Temkin isotherm models respectively.

$$\ln q_e = \ln K_f + \frac{1}{n} \ln C_e \quad (3)$$

$$\frac{1}{q_e^2} = \frac{B_{HJ}}{A_{HJ}} - \frac{1}{A_{HJ}} \text{Log} C_e \quad (4)$$

$$\ln q_e = \ln q_{max} + K_j \ln C_e \quad (5)$$

$$q_e = K_1 \ln K_2 + K_1 \ln C_e \quad (6)$$

The Table 3 shows the dependent and independent variables plotted to obtained the respective slope and intercept for each isotherm model. The obtained slopes and intercepts were subsequently used to calculate the various isotherm parameters required to explain the adsorption of Cu and Fe ions.

Table 3 shows the Freundlich constants ( $K_f$ ) as the adsorption capacities of the prepared adsorbents for Cu and Fe ions. The higher adsorption capacities of both adsorbents for Fe ions compare to Cu ions can be explained by their higher af-

**Tables 4:** Isotherm models parameters for the adsorption of Cu and Fe ions using CHS and COMP.

Isotherm Models	CHS		COMP	
	Metals		Metals	
Jovanovic	Cu	Fe	Cu	Fe
$K_j$	0.348	0.211	0.348	0.218
$q_{max}$	7.907	11.900	7.905	11.905
$R^2$	0.999	0.999	0.999	0.977
Standard error	$6.0 \times 10^{-4}$	$2.34 \times 10^{-6}$	$4.0 \times 10^{-4}$	0.068
Freundlich				
$K_f$	6.402	11.759	6.377	10.907
N	-11.620	-515.464	-11.232	-39.154
$R^2$	0.959	0.856	0.988	0.919
Standard error	$7.5 \times 10^{-3}$	$1.1 \times 10^{-3}$	$4.0 \times 10^{-3}$	$7.17 \times 10^{-3}$
Temkin				
$K_1$	-0.620	-0.023	-0.641	-0.352
$K_2$	$3.5 \times 10^{-5}$	$1.2 \times 10^{-22}$	$5.16 \times 10^{-5}$	$6.35 \times 10^{-28}$
$R^2$	0.966	0.856	0.990	0.954
Standard error	0.0494	0.0129	0.0264	0.0582
Harkins-Jura				
$A_{HJ}$	-130.513	$-1.6 \times 10^4$	-126.326	-1127.39
$B_{HJ}$	-3.114	-113.961	-3.033	-9.433
$R^2$	0.946	0.855	0.984	0.911
Standard error	$3.4 \times 10^{-3}$	$1.56 \times 10^{-5}$	$2.0 \times 10^{-4}$	$1.0 \times 10^{-4}$

**Table 5:** Kinetic models for Cu and Fe ions removal from electroplating wastewater using CHS and COMP.

Kinetic Models	CHS		COMP	
	Metals		Metals	
Pseudo-first order	Cu	Fe	Cu	Fe
$K_1$	$5.33 \times 10^{-4}$	$1.27 \times 10^{-3}$	$1.33 \times 10^{-3}$	$3.76 \times 10^{-3}$
$R^2$	0.918	0.843	0.758	0.789
Standard error	0.004	0.003	0.021	0.053
Pseudo-second order				
$K_2$	$2.40 \times 10^{-4}$	$2.90 \times 10^{-4}$	$5.60 \times 10^{-4}$	$9.40 \times 10^{-4}$
$R^2$	0.918	0.847	0.766	0.771
Standard error	0.004	0.003	0.001	0.014
Elovich				
$\Delta$	21.7200	5.0300	9.600	1.630
$\Theta$	$2.27 \times 10^{18}$	$1.63 \times 10^7$	$1.41 \times 10^7$	14.700
$R^2$	0.972	0.777	0.595	0.950
Standard error	0.006	0.078	0.063	0.104
Intraparticle diffusion				
$K_{int}$	0.015	0.069	9.600	0.200
L	2.156	3.903	$1.41 \times 10^7$	2.892
$R^2$	0.956	0.814	0.595	0.997
Standard error	0.007	0.071	0.001	0.006

finities for Fe ions in aqueous media [38]. Moreover, the high values of  $K_f$  for both adsorbents in this study may be due to the large number of binding sites in the CHS and the large surface area of the COMP.

The constants correlation coefficients ( $R^2$ ) and standard errors of the four selected adsorption isotherms are shown in Table 3. It is evident that adsorptions mechanism of the Cu and Fe ions by CHS and CHS-silver nanocomposite fitted well to the Jovanovic isotherm model than other isotherm models tested which is based on its very high correlation coefficients approximately 1 and very low standard errors close to 0. Thus, equilibrium data for the Cu and Fe adsorption onto CHS and CHS-silver nanocomposite fitted well into the isotherm models in the following order: Jovanovic > Harkin-Jura > Freundlich > Temkin.

**Kinetic model of Cu and Fe ions adsorption:** In the adsorption studies, mechanism and rate of adsorption of Cu and Fe ions by CHS and COMP were analyzed by applying different kinetic models. These models include Elovich, pseudo-first order, pseudo-second order and intraparticle models. Table 4 shows the values of the rate constants and other parameters obtained from the slopes and intercepts of the plots. The equations for these kinetic models were shown as equations 7, 8, 9 and 10.

Pseudo-first order equation

$$\ln[C] = \ln[C_0] - kt \quad (7)$$

Pseudo - second order kinetic model

$$\frac{1}{[C]} = \frac{1}{[C_0]} + kt \quad (8)$$

Elovich kinetic model

$$C = \frac{1}{\delta} \ln(\theta\delta) + \frac{1}{\delta} \ln(t) \quad (9)$$

Intraparticle kinetic model

$$q_t = K_i t^{1/2} + C \quad (10)$$

From Table 5, it can be seen that the standard errors of Pseudo-second order model for the removal of the selected metal ions on both adsorbents were lower compare to other kinetic models tested. This suggests that Pseudo-second order kinetic model better described adsorption kinetics of Cu and Fe onto CHS. The Pseudo-second order rate constants  $K_2$  (Table 5) for the adsorption of Fe were found to be higher compare to that of Cu, which supports that the uptake of Fe ions by both adsorbents was more favourable. This outcome agreed with results reported by Arshadi, *et al.* [39] and Meitei and Prasad [40]. In addition, Table 5 shows that the values of Elovich constants are high; this implies increase in adsorption rate. Also, to explain the absence of metal ions removal on heterogeneous surfaces, the kinetic data did not fit onto Elovich kinetic model [41].

**Thermodynamic studies of the Cu and Fe ions removal:**

The nature of an adsorption process can be derived from thermodynamic studies. The set parameters are the Gibbs energy ( $\Delta G^\circ$ ), changes in enthalpy ( $\Delta H^\circ$ ) and changes in entropy ( $\Delta S^\circ$ ).  $\Delta G^\circ$  indicates the spontaneity of the adsorption. So, negative value of  $\Delta G^\circ$  at a certain temperature indicates spontaneous adsorption. The  $\Delta G^\circ$  of adsorption process is usually determined by Van't Hoff equation (Equation 11) [42]:

$$\Delta G^\circ = -RT \ln K \quad (11)$$

Equation 12 shows the relationship between  $\Delta H^\circ$ ,  $\Delta S^\circ$  and  $\Delta G^\circ$ , while after substitution of Equation 11 into Equation 12, the relationship between equilibrium constant and temperature is presented as Equation 13.

$$\Delta G^\circ = -RT \ln K = \Delta H^\circ - T \Delta S^\circ \quad (12)$$

**Table 6:** Gibbs free energy (KJ/mol), Enthalpy change (KJ/mol) and Entropy Change (KJ/molK) for the removal of Cu and Fe ions on CHS and COMP.

Adsorbent	Temperature (K)	Heavy metal ions	
		Cu	Fe
CHS	303	-1.401	-1.731
	318	-1.607	-1.825
	333	-1.695	-1.914
	348	-1.868	-2.005
	363	-1.804	-2.091
COMP	303	-1.484	-1.619
	318	-1.576	-1.718
	333	-1.787	-1.830
	348	-1.898	-1.991
	363	-1.932	-2.057
CHS	$\Delta H$	0.781	0.111
	$\Delta S$	0.007	0.006
COMP	$\Delta H$	1006.376	853.350
	$\Delta S$	8.233	8.120

$$\ln K = \frac{-\Delta H^\circ}{RT} + \frac{\Delta S^\circ}{R} \quad (13)$$

Where K and R represent equilibrium and gas constants respectively

The slope and intercept of the plot of  $\ln K$  against  $1/T$  as a straight line were used to calculate the values of  $\Delta H^\circ$  and  $\Delta S^\circ$  respectively. The Table 6 shows that positive  $\Delta H^\circ$  values for the adsorption of Cu and Fe ions by both CHS and COMP were obtained. This indicates that the adsorption of these metals is endothermic [43]. The  $\Delta S^\circ$  describes the degree of randomness during adsorption process. The positive values of  $\Delta S^\circ$  in Table 6 show that randomness at the adsorbent-solution interface increase and also, the affinity of the adsorbents for the metal ions was enhanced [44,45].

Table 6 shows the negative  $\Delta G^\circ$  values for the removal of Cu and Fe ions in CHS and COMP which indicate that the adsorption processes were feasible and spontaneous. It was also noticed that as temperature increases, the  $\Delta G^\circ$  values decrease indicating favourable adsorption at elevated temperatures [46].

## Conclusion

Preparation of nanocomposite of CHS and silver nanoparticles was successful. Both the CHS and its nanocomposite proved to be effective adsorbents for the removal of Cu (II) and Fe (II) ions from electroplating wastewater. The presence of functional groups revealed by FTIR spectrum as active sites in this adsorbent helped to bind Cu (II) and Fe (II) ions on the adsorbent surface. The adsorptions of the selected metal ions depend on contact time, adsorbent dose and temperature. Also, the results shown Jovanovic isotherm model best fitted the removal of Cu and Fe ions. The Pseudo-second kinetic model was a better model for their adsorption. Therefore, it is believed that this nanocomposite as an adsorbent can serve as an inexpensive alternative to remove heavy metals from electroplating wastewater.

## Acknowledgments

Financial support received from Tertiary Education Trust Fund (TETFUND) Nigeria with grant number TETFUND/FUT-MINNA/2016-2017/6<sup>th</sup> BRP/05 is very much appreciated.

## References

1. Tchounwou PB, Yedjou CG, Patlolla AK, et al. (2012) Heavy metal toxicity and the environment. *EXS* 101: 133-164.
2. Ezzat AK, Algharib AM (2013) Removal of strontium from industrial wastewater using capsules and leaves of castor bean and jojoba plants. *Zagazig Journal of Agricultural Research* 40: 10-22.
3. Yao-Jen T, Chen-Feng Y, Zhonghao Z, et al. (2014) Strontium removal in seawater by means of composite magnetic nanoparticles derived from industrial sludge. *Water* 8: 357.
4. Sivasangari S, Suseendhar S, Suresh K, et al. (2016) Characteristic study of electroplating and dye industrial effluents. *International Journal of Innovative Research in Science, Engineering and Technology* 5: 2319-8753.
5. Barakat MA (2011) New trends in removing heavy metals from industrial wastewater. *Arabian Journal of Chemistry* 4: 361-377.
6. Khulbe KC, Matsuura T (2018) Removal of heavy metals and pollutants by membrane adsorption techniques. *Applied Water Science* 8: 19.
7. Akolo SA, Kovo AS (2015) Comparative study of adsorption of copper ion onto locally developed and commercial chitosan. *Journal of Encapsulation and Adsorption Sciences* 5: 21-37.
8. Opeolu BO, Bamgbose O, Arowolo T, et al. (2010) Utilization of biomaterials as adsorbents for heavy metals' removal from aqueous matrices. *Scientific Research and Essays* 5: 1780-1787.
9. GangSeob J, Zhao Q, Markus JB (2015) Mechanical properties and failure of biopolymers: Atomistic reactions to macroscale response. *Top Curr Chem* 369: 317-343.
10. Maduka HCC, Ugwu CE, Okpogba AN, et al. (2015) The efficacy of chitosan obtained from Nigerian snail shell for the treatment of waste water effluent. *Journal of Biodiversity and Environmental Sciences* 7: 9-15.
11. Zhitong Y, Meisheng X, Haiyan L, et al. (2014) Bivalve shell: Not an abundant useless waste but a functional and versatile biomaterial. *Critical Reviews in Environmental Science and Technology* 44: 2502-2530.
12. Sobhanardakani S, Zandipak R, Parvizimosaed H, et al. (2014) Efficiency of chitosan for the removal of Pb (II), Fe (II) and Cu (II) ions from aqueous solutions. *Iranian Journal of Toxicology* 8: 1145-1151.
13. Sotiriou GA, Sannomiya T, Teleki A, et al. (2010) Non-toxic dry-coated nanosilver for plasmonic biosensors. *Advanced Functional Material* 21: 4250-4257.
14. Hajji S, Younes I, Ghorbel-Bellaaj O, et al. (2014) Structural differences between chitin and chitosan extracted from three different marine sources. *International Journal Biology and Macromolecules* 65: 298-306.
15. Wang Y, Pitto-Barry A, Habtemariam A, et al. (2016) Nanoparticles of chitosan conjugated to organo-ruthenium complexes. *Inorganic Chemistry Frontier* 3: 1058-1064.
16. Ahmad MB, Lim JJ, Shameli K, et al. (2011) Synthesis of silver nanoparticles in chitosan, gelatin and chitosan/gelatin bionanocomposites by a chemical reducing agent and their characterization. *Molecules* 16: 7237-7248.
17. Shameli K, Ahmad M B, Zargar M (2011) Synthesis and characterization of silver/montmorillonite/chitosan bionanocomposites by chemical reduction method and their antibacterial activity. *Int J Nanomedicine* 6: 271-284.
18. Astalakshmi A, Nima P, Ganesan V (2013) A green approach in the synthesis of silver nanoparticles using bark of Eucalyptus globulus, Labill. *International Journal of Pharmaceutical Sciences Review and Research* 23: 47-52.
19. Gunatilake SK (2015) Methods of removing heavy metals from industrial wastewater. *Journal of Multidisciplinary Engineering Science Studies* 1: 1-7.
20. Bao Q, Dun Z, Peng Q (2011) Synthesis and characterization of silver nanoparticle and graphene oxide nanosheet composites as a bactericidal agent for water disinfection. *Journal of Colloid and Interface Science* 360: 463-470.
21. Mie R, Samsudin MW, Din LB, et al. (2014) Synthesis of silver nanoparticles with antibacterial activity using the lichen *Parmotrema praesorediosum*. *International Journal of Nanomedicine* 9: 121-127.

22. Jain S, Mehata MS (2017) Medicinal plant leaf extract and pure flavonoid mediated green synthesis of silver nanoparticles and their enhanced antibacterial property. *Scientific Reports* 7: 15867.
23. Thien DT, An NT, Hoa NT (2015) Preparation of fully deacetylated chitosan for adsorption of Hg (II) ion from aqueous solution. *Chemical Science Journal* 6.
24. Razzaz A, Ghorban S, Hosayni L, et al. (2016) Chitosan nanofibers functionalized by TiO<sub>2</sub> nanoparticles for the removal of heavy metal ions. *Journal of the Taiwan Institute of Chemical Engineers* 58: 333-343.
25. Maciel V, Yoshida C, Pereira S, et al. (2017) Electrostatic self-assembled chitosan-pectin nano- and microparticles for insulin delivery. *Molecules* 22: 1707.
26. Pervez MN, Stylios GK (2018) Investigating the synthesis and characterization of a novel "Green" H<sub>2</sub>O<sub>2</sub>-assisted, water-soluble chitosan/polyvinyl alcohol nanofiber for environmental end uses. *Nanomaterials (Basel)* 8: 395.
27. Zhang X, Liu Z, Shen W, et al. (2016) Silver nanoparticles: Synthesis, characterization, properties, applications, and therapeutic approaches. *International Journal of Molecular Sciences* 17: 1534.
28. Krishnaveni B, Ragunathan R (2015) Extraction & characterization of chitin and chitosan from *Bionetria CBNR BKRR*, synthesis of their bionanocomposites and study of their application. *Indo Global Journal of Pharmaceutical Sciences* 5: 40-52.
29. Khalid MH, Pervez MF, Uddin MJ, et al. (2018) Influence of natural dye adsorption on the structural, morphological and optical properties of TiO<sub>2</sub> based photoanode of dye-sensitized solar cell. *Materials Science-Poland* 36: 93-101.
30. Das B, Mondal NK, Bhaumik R, et al. (2014) Insight into adsorption equilibrium, kinetics and thermodynamics of lead onto alluvial soil. *International Journal Environmental Science Technology* 11: 1101-1114.
31. Kaveeshwar A, Sanders M, Ponnusamy SK, et al. (2017) Chitosan as a biosorbent for adsorption of iron (II) from fracking wastewater. *Polymers for Advanced Technologies* 29: 961-969.
32. Gupta VK, Agarwal S, Saleh TA (2011) Synthesis and characterization of alumina-coated carbon nanotubes and their application for lead removal. *Journal of Hazardous Material* 185: 17-23.
33. Bankole MT, Abdulkareem AS, Mohammed IA, et al. (2019) Selected heavy metals removal from electroplating wastewater by purified and polyhydroxybutyrate functionalized carbon nanotubes Adsorbent. *Scientific Reports* 9: 4475.
34. Priyanka T, Mahesh CV, Sushil KJ, et al. (2017) Adsorption of Pb (II), Cu (II), and Zn (II) ions onto *urtica dioica* leaves (UDL) as a low cost adsorbent: Equilibrium and thermodynamic studies. *Modern Chemistry* 5: 11-18.
35. Hakan D, Cihan G (2016) Adsorption of copper (II) from aqueous solutions on activated carbon prepared from grape bagass. *Journal of Cleaner Production* 124: 103-113.
36. Areco MM, Afonso MS (2010) Copper, zinc, cadmium and lead biosorption by *Gymnogongrus torulosus*. Thermodynamics and kinetics studies. *Biointerfaces* 81: 620-628.
37. Md Sayedur R, Kathiresan VS (2015) Heavy metal adsorption onto *Kappaphycus sp.* from aqueous solutions: The use of error functions for validation of isotherm and kinetics models. *BioMed Research International* 2015.
38. Arivoli S, Marimuthu V, Mohamed ARJ (2013) Kinetics of batch adsorption of iron (II) ions from aqueous solution using activated carbon from *Strychnos Nux-Vomica L.* *International Journal of Scientific and Engineering Research* 4: 407-417.
39. Arshadi M, Amiri MJ, Mousavi S (2014) Kinetic, equilibrium and thermodynamic investigations of Ni (II), Cd (II), Cu (II) and Co (II) adsorption on barley straw ash. *Water Resources and Industry* 6: 1-17.
40. Meitei MD, Prasad MNV (2014) Adsorption of Cu (II), Mn (II) and Zn (II) by *Spirodela polyrhiza* (L.) schleiden: Equilibrium, kinetic and thermodynamic studies. *Ecological Engineering* 71: 308-317.
41. Enos WW, Stephen A, Paul MS, et al. (2018) Removal of heavy-metals from wastewater using a hydrous alumino-silicate mineral from Kenya. *Bulletin of Chemical Society of Ethiopia* 32: 39-51.
42. Rathod M, Mody K, Basha S (2014) Efficient removal of phosphate from aqueous solutions by red seaweed, *Kappaphycus alvarezii*. *Journal of Cleaner Production* 84: 484-493.
43. Murthy CR, Ramesh P, Ramesh A (2011) Study of biosorption of Cu (II) from aqueous solutions by coconut shell powder. *Chemical Science Journal* 17: 1-15.
44. Maksin DD, Kljajević SO, Dolić MB (2012) Kinetic modelling of heavy metal sorption by vinyl pyridine based copolymer. *Hem Ind* 66: 795-804.
45. Somasundaram S, Sekar K, Gupta VK, et al. (2013) Synthesis and characterization of mesoporous activated carbon from rice husk for adsorption of glycine from alcohol-aqueous mixture. *Journal of Molecular Liquids* 177: 416-425.
46. Hamideh R, Ali AG, Habibollah Y, et al. (2012) Adsorption of Fe (II) ions from aqueous phase by chitosan adsorbent: Equilibrium, kinetic, and thermodynamic studies. *Desalination and Water Treatment* 50: 348-359.

DOI: 10.36959/742/228